Journal of Materials Chemistry

Cite this: *J. Mater. Chem.*, 2012, **22**, 6639

www.rsc.org/materials

PAPER

Magnetic core–shell-structured nanoporous organosilica microspheres for the Suzuki–Miyaura coupling of aryl chlorides: improved catalytic activity and facile catalyst recovery†

Hengquan Yang,* Guang Li and Zhancheng Ma

Received 6th November 2011, Accepted 30th January 2012
DOI: 10.1039/c2jm15693h

New magnetic core–shell-structured nanoporous organosilica microspheres consisting of a Fe_3O_4 core and an organosilica shell with a built-in N-heterocyclic carbene (NHC) moiety were synthesized through surfactant-directed self-assembly on surface. The structure and composition of the material thus-designed were confirmed by N_2 sorption, XRD, TEM, FT-IR, *etc*. Such composite microspheres possess highly open mesopores (1.6 nm) in the shell, moderate surface area, tunable shell thickness, uniform morphology, high magnetization as well as good coordination ability toward Pd. The catalytic activity test with the Suzuki–Miyaura couplings of challenging aryl chlorides reveals that this Pd-coordinated material is highly active for a wide range of substrates, suggesting highly promising application potentials of the magnetic core–shell-structured nanoporous organosilica. In particular, the catalyst derived from this material is superior to NHC-functionalized MCM-41 microspheres and a commercial Pd/C catalyst in terms of activity and recovery. The catalytic activity enhancement effects may be attributable to the purposely designed core–shell structure with significantly decreased diffusion depth, which is crucial for designing high-performance solid catalysts.

Introduction

Currently, core–shell microspheres are attracting extensive attention because the ready adjustability and functionality, both of the cores and the shells, can confer them with a wide number of potential applications in catalysis, drug delivery, biosensor, and so forth.[1] Of various core–shell structured microspheres, magnetic porous silica microspheres consisting of a magnet core and a nanoporous silica shell are of particular interest owing to the unusual properties that, in addition to a magnet-responsive function, the nanoporous silica shell can provide a versatile platform for designing more sophisticated materials.[2] For example, Shi and co-workers synthesized magnetic core–shell-structured nanoporous silica nanospheres, which exhibited excellent performances in drug delivery.[3] Zhao' group prepared multifunctional microspheres comprised of a core of Au-supported Fe_3O_4–silica composite and an outer shell of ordered nanoporous silica with perpendicularly aligned pore channels.[4] This multifunctional microsphere were highly active in the reduction of 4-nitrophenol and styrene epoxidation. Yin *et al.* fabricated a magnetic Au catalyst by encapsulation of a core–satellite composite within a porous silica shell.[5] This material exhibited an excellent catalytic stability. Yang's group trapped Au nanoparticles in yolk–shell-structured organosilica microspheres, which exhibited high acidity in the reduction of 4-nitrophenol.[2h] Obviously, the development of multifunctional magnetic porous microspheres has made exciting progress and they exhibit highly promising potential applications. However, in contrast to the ever-expanding intended applications that often require porous silica with specific organic or inorganic functionalization, thus providing properties not obtainable from pure silica, the applications of catalytically active magnetic core–shell nanoporous silica microspheres are rather limited.

Over the past few years, mesoporous organosilicas, synthesized through co-condensation of organic moiety-bridged trialkoxysilane and tetraalkoxysilane with the aid of templates in one pot, have also aroused considerable interest in the fields of catalysis, sorption and drug delivery due to their high surface, large pore volume and tunable pore sizes.[6] Compared with the organo-modified mesoporous silica prepared by post grafting, mesoporous organosilica usually has a larger surface area, higher pore volume and less diffusion resistance because of the incorporation of organic moieties in the framework instead of their being grafted on the pore surface. Moreover, organic moieties are more homogeneously distributed in the framework of the materials thanks to the self-assembly at the molecular level. Salen complex-, tartardiamide-, binol-, imidazolium-, alkyl- and

School of Chemistry and Chemical Engineering, Shanxi University, Taiyuan 030006, P. R. China. E-mail: hqyang@sxu.edu.cn; Fax: +86-351-7011688; Tel: +86-351-7010588

† Electronic supplementary information (ESI) available: The TEM images, XRD pattern of NHC-functionalized MCM-41, photograph of magnetic isolation and ^{1}H NMR data of the coupling products. See DOI: 10.1039/c2jm15693h

aryl-functionalized mesoporous organosilicas, to name a few, were successfully prepared and showed promising performances in catalysis.[6e,7] However, the conventional synthesis protocols usually lead to mesoporous organosilicas with non-uniform morphology and/or particle size as large as several hundred nanometres to micrometres. The diffusion limitation phenomena caused by the long nano-channels in the large particles are often observed. The activity of a complex catalyst immobilized on a mesoporous material is generally much lower than the free complex catalyst in solution.[8]

Decreasing particle sizes down to the nanoscale may be an effective way to mitigate the diffusion limitations because the diffusion lengths of reactant molecules are dramatically shortened. However, when the particle sizes are less than 100 nm, the isolation of these nanoparticles from a reaction system is relatively difficult and time-consuming because of the unavoidable need for high speed centrifugation. The diffusion limitations and catalyst recovery might be simultaneously addressed if the catalytically active part was positioned surrounding magnetic nanospheres (resulting in a multifunctional core–shell structure) and the catalytic reaction thus occurs only in the outer nanoporous shell instead of throughout the solid material. However, to the best of our knowledge, there has been no report on the preparation and catalytic applications of magnetic core–shell-structured nanoporous organosilica microspheres with a built-in active phase only in the shell.

Our recent efforts have focused on development of recoverable solid catalysts for the Suzuki–Miyaura coupling reaction as it is a fundamental reaction for synthesizing fine chemicals.[9] Particular attention is paid to the use of aryl chlorides as substrates because they are much cheaper and readily available than the usually used aryl bromides and iodides. However, the catalytic activation of aryl chlorides is considerably challenging especially for heterogeneous catalysts. So far, heterogeneous examples for the Suzuki–Miyaura coupling of less reactive aryl chlorides are quite rare.[10] In our recent work, we have successfully developed active solid catalysts for this reaction by incorporation of NHC (*N*-heterocyclic carbene, the most successful class of ligands in recent organometallic chemistry) into the framework of the mesoporous material.[7c,7d] However, the coupling reactions over the resulting solid catalysts proceeded relatively sluggishly. It required 24 h to achieve satisfactory yields and its activity was much lower than that of the homogeneous counterpart.[7c] There is a significant need to improve the catalytic activity.

In this context, combining the merits of magnetic particles, the core–shell structure and nanoporous organosilica in a single system will probably create a high-performance multifunctional solid catalyst for the Suzuki–Miyaura coupling of challenging substrates. In light of this idea, we herein demonstrate a novel appraoch for the synthesis of new magnetic composite microspheres consisting of a Fe_3O_4 core and a nanoporous organosilica shell with the built-in bulky NHC ligand, and we investigate their ability in coordinating metals, and further examine their catalytic performances. Interestingly, the Pd-coordinated material exhibits activity enhancement effects in the Suzuki–Miyaura coupling of aryl chlorides as compared to NHC-functionalized MCM-41 microspheres possibly due to the significantly shortened diffusion depth. Although magnetic core–shell silica microspheres have been reported,[2] we proceed be outlining the synthesis of new magnetic core–shell-structured *organosilica* microspheres with molecular functionalization in the shell and disclose their unusual properties.

Experimental

Reagents and materials

$Pd(acac)_2$ (acac = acetylacetonate) were obtained from Kaida Metal Catalyst & Compounds Co. Ltd (China). Various arylboronic acids were bought from Beijing Pure Chemical Co. Ltd. Pd/C catalyst (1 wt% Pd) was purchased from the Aladdin Company. Most of the aryl chlorides, ICl, $FeCl_3$, tetraethyl orthosilicate (TEOS) and cetyltriethylammonium bromide (CTAB) were purchased from the Aladdin Company. 2,6-Diisopropylaniline, concentrated ammonia solution (28 wt%) and other reagents were obtained from Shanghai Chemical Reagent Company of Chinese Medicine Group. 1,3-Bis(4-triethoxysilyl-2,6-diisopropylphenyl)-imidazol-3-iumtrifluorometh-ane-sulfonate (NHC-bridged organosilane) was synthesized according to our previous publication.[7c]

Synthesis of magnetic NHC-functionalized nanoporous organosilica

Fe_3O_4 particles were synthesized according to the reported method.[11] 0.4 g of Fe_3O_4 particles was dispersed in 200 mL of 0.1 mol HCl and was subject to ultrasonic treatment. After 10 min, this material was washed with water and isolated with the aid of a magnet. The resultant material was re-dispersed into a mixture solution (320 mL of ethanol, 80 mL of water and 4.2 mL of concentrated ammonia solution). Under stirring, 0.12 g of tetraethyl orthosilicate (TEOS) was added into the mixture solution. After this mixture was further stirred for 6 h at room temperature, the resultant solid was separated, repeatedly washed with ethanol and dried under air, eventually leading to SiO_2-coated Fe_3O_4 particles.

0.5 g of SiO_2-coated Fe_3O_4 particles were dispersed in 250 mL of 0.1 mol L^{-1} HCl solution which was then treated under ultrasonic conditions.[4] After 10 min, the SiO_2-coated Fe_3O_4 was separated with a magnetic field, and then repeatedly washed with distilled water. Next, ethanol (380 mL), water (400 mL), concentrated ammonia solution (5.0 g, 28 wt%) and CTAB (1.5 g) were admixed with the resultant SiO_2-coated Fe_3O_4. After the solution was stirred at 35 °C for 5 h, total 4.75 mmol of the total siliceous precursors dissolved in 3 mL of ethanol was added dropwise to the above system. The molar fraction of NHC-bridged organosilane in the total siliceous precursors was 5.26%. The mixture was further vigorously stirred for 10 h. The resultant microspheres were separated with a magnet. CTAB infiltrated in the shell nanopores was removed by repeated acetone extractions under reflux conditions. After being dried under vacuum, the magnetic composite microspheres were eventually obtained, denoted as Fe_3O_4@mSiO_2-NHC(x) where x depended on the following synthesis conditions. To obtain the composite with different shell thicknesses, the total amount of added siliceous precursors including TEOS and NHC-bridged organosilane (the molar ratios of NHC-bridged organosilane and TEOS were always kept constant at 5.26%) was varied from 4.75 mmol to 3.562 and 2.375 mmol. According to the added amount of

siliceous precursor, we obtained three materials corresponding to Fe_3O_4@mSiO_2-NHC(1), Fe_3O_4@mSiO_2-NHC(2) and Fe_3O_4@mSiO_2-NHC(3), respectively.

For comparison, we synthesized NHC-functionalized MCM-41 microspheres without Fe_3O_4 core. In a typical synthesis, 3.52 g of CTAB and 2.5 mL of 1 mol L^{-1} sodium hydroxide solution were dissolved in 800 g of a mixture of methanol and water (50/50, w/w). Next, 3 mL of methanol containing 8.684 mmol of TMOS and 0.0482 mmol of NHC-bridged organosilane was loaded to the solution with vigorous stirring at 298 K. After further stirring for 8 h hours at this temperature, the resulting white precipitate was isolated by filtration and thoroughly washed with distilled water. The template was removed through the same procedure as with Fe_3O_4@mSiO_2-NHC(1).

Coordination of Fe_3O_4@mSiO_2-NHC(x) with $Pd(acac)_2$

In a typical experiment, 1 g of Fe_3O_4@mSiO_2-NHC(1) (dried at 120 °C for 4 h) was dispersed in 12 mL of dry 1,4-dioxane containing 0.0063 g of $Pd(acac)_2$ (acac = acetylacetonate). After the mixed system was stirred at 100 °C for 30 h under N_2 atmosphere, the magnetic solid was collected by employing a magnetic field. The solid was repeatedly washed with dry 1,4-dioxane and dried under vacuum for the catalysis tests. As for Fe_3O_4@mSiO_2-NHC(2) and Fe_3O_4@mSiO_2-NHC(3), the amounts of $Pd(acac)_2$ were decreased to 0.0053 and 0.0041 g without changing any other conditions, respectively. The molar ratio of NHC/Pd was kept the same.

General procedure for the Suzuki–Miyaura coupling

A mixture of aryl chlorides (2.0 mmol), phenylboronic acid (2.2 mmol), potassium *tert*-butoxide (3 mmol) and *iso*-propyl alcohol (6 mL), and the solid catalyst (0.5 mol% with respect to aryl chlorides) were stirred at 80 °C under an N_2 atmosphere for a given time. At the end of reaction, the mixture was cooled to room temperature and was repeatedly extracted with diethyl ether. The combined organic layers were concentrated and the resulting product was purified by a column chromatography on silica gel. The product was confirmed by ^{1}H NMR (see the ESI†). Its purity was confirmed by GC.

The recycling test for the Suzuki–Miyaura coupling was conducted as follows. At the end of the first run, the mixture was cooled to room temperature and the liquid was isolated with aid of an external field. The recovered catalyst was washed with diethyl ether, water, methanol and acetone in sequence and then dried under vacuum. The recovered catalyst was weighed again. Fresh solvent and substrates were added, but the molar ratio of substrate to Pd remained the same as that in the first run.

The procedures for the coupling reactions of benzyl chloride and arylboronic acids were the same as those of aryl chlorides.

Characterization and analysis

Wide-angle powder X-ray powder diffraction was performed on a Rigaku D/Max 3400 powder diffraction system. N_2 physical adsorption was carried out on a micrometritics. ASAP2020 volumetric adsorption analyzer (before measurements, samples were out gassed at 125 °C for 6 h). The Brunauer–Emmett–Teller (BET) surface area was evaluated from data in the relative pressure range of 0.05 to 0.15. The total pore volume of each sample was estimated from the amount adsorbed at the highest P/P_0 (*ca.* 0.99). Magnetization measurements $M(T,H)$ were performed by using a superconducting quantum interference device magnetometer (LakeShore 7410). FT-IR spectra were collected on a PE-1730 infrared spectrometer infrared spectrometer. Pd content was analyzed with an inductively coupled plasma-atomic emission spectrometry (ICP-AES, AtomScan16, TJA Co.). X-Ray photoelectron spectra (XPS) were recorded on a Kratos Axis Ultra DLD, and the C_{1S} line at 284.8 eV was used as a reference. TEM micrographs were taken with a JEM-2000EX transmission electron microscope. GC analysis was conducted on a SP-GC6800A.

Results and discussion

Material synthesis

In order to integrate the NHC moiety with the framework of shell, we introduced two hydrolysable triethoxysilyl groups onto the terminals of the NHC ligand to obtain an NHC-bridged organosilane (1,3-bis(4-triethoxysilyl-2,6-diisopropylphenyl)-imidazol-3-ium-trifluoro-methane sulfonate). The synthesis of NHC-bridged triethoxysilane was reported in our recent publications.[7c] The fabrication of magnetic core–shell-structured nanoporous organosilica microspheres consists of four steps according to the modified method,[4] as described in Scheme 1. Firstly, the Fe_3O_4 microspheres were prepared according to the reported method.[4] In order to a grow uniform nanoporous shell around the Fe_3O_4 core and to protect Fe_3O_4 core under harsh conditions, the Fe_3O_4 microspheres with a rough surface were first coated with a thin layer of SiO_2. Next, a NHC-functionalized nanoporous organosilica shell was created surrounding silica-coated Fe_3O_4 cores through a sol–gel process in the presence of CTAB as template. After removing CTAB infiltrated in the shell nanopores, the magnetic core–shell nanoporous organosilica microspheres with built-in NHC moieties were eventually obtained. By gradually reducing the amount of the added siliceous precursors in the third step, we expected to achieve three samples with gradually decreasing shell thicknesses:

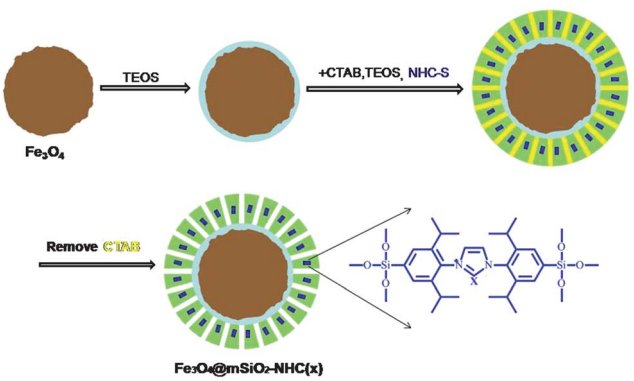

Scheme 1 Schematic description for the synthesis of Fe_3O_4@mSiO_2-NHC(x), HNC–S = 1,3-bis(4-triethoxysilyl-2,6-diisopropylphenyl)-imiadzol-3-ium-trifluoro-methane sulfonate (NHC-bridged organosilane).

Fe_3O_4@mSiO_2-NHC(1), Fe_3O_4@mSiO_2-NHC(2) and Fe_3O_4@mSiO_2-NHC(3).

Structural characterization

We employed N_2 physical sorption, XRD and TEM to check the structures of the synthesized samples. N_2 adsorption/desorption isotherms of these materials are shown in Fig. 1, and the physical parameters measured with N_2 sorption are summarized in Table 1. The sample Fe_3O_4@mSiO_2-NHC(1) shows a type-IV isotherms, suggesting the presence of cylindrical nanopores. The surface area, pore volume and pore size were determined to be 216 m^2 g^{-1}, 0.13 cm^3 g^{-1} and 1.6 nm, respectively. The values obtained for surface area and pore volume per unit mass of Fe_3O_4@mSiO_2-NHC(1) are large, especially considering that the total mass of the sample is dominated by the contribution from the nonporous Fe_3O_4 core. The surface areas of a typical mesoporous material which has a fully porous structure are as large as 600–1000 m^2 g^{-1} and pore volume as high as 0.5–1.0 cm^3 g^{-1} depending on the synthetic conditions. The striking contrast is suggestive of a fact that the obtained Fe_3O_4@mSiO_2-NHC(1) has a fractionally porous architecture. The determined pore size of this sample is much smaller than that of typical MCM-41, which is caused by the presence of a larger amount of ethanol in the synthesis system and bulky NHC moieties present on the nanopore surface.[12] Fe_3O_4@mSiO_2-NHC(2) also shows type-IV isotherms, but their surface area and pore volume have apparently decreased. The same trend was observed for the Fe_3O_4@mSiO_2-NHC(3) sample. The decreases in these parameters reflect the decrease in the fraction of the porous shell in the whole material, which is due to the reduction in the amount of siliceous precursor added. The dependence of the physical properties on the amount of added siliceous precursor confirms that the structural aspects of these materials can be tunabed.

The XRD patterns of these three materials are shown in Fig. 2. One diffraction peak at $2\theta = 2.4°$ was clearly observed for Fe_3O_4@mSiO_2-NHC(1), confirming a somewhat ordered organization of the architecture. This diffraction peak can be attributed to the (100) plane if the pore structure was assigned to the MCM-41 family. The (110) and (200) diffraction peaks that were usually observed in a standard MCM-41 sample, were not found. This can be explained by the fact that the presence of the bulky organosilane affects the interactions between silicon oligomers and template molecules and the assembly ability is thus discounted. The intensity of (100) diffraction peaks gradually decrease in the order of Fe_3O_4@mSiO_2-NHC(1), Fe_3O_4@mSiO_2-NHC(2), and Fe_3O_4@mSiO_2-NHC(3), probably reflecting a gradual decrease in the shell thickness.

Table 1 Physical parameters of the synthesized magnetic core–shell organosilica microspheres

Samples	S^a (m^2 g^{-1})	P^b (cm^3 g^{-1})	D^c (nm)
Fe_3O_4@mSiO_2-NHC(1)	216	0.13	1.6
Fe_3O_4@mSiO_2-NHC(2)	163	0.11	1.6
Fe_3O_4@mSiO_2-NHC(3)	120	0.08	1.7

[a] BET surface area. [b] Single point pore volume calculated at a relative pressure P/P_0 of 0.99. [c] Calculation from adsorption branch.

The TEM images of the samples with low and high magnifications are displayed in Fig. 3. TEM images clearly show that the prepared Fe_3O_4 sample consists of monodispersed microspheres with diameters of about 200 nm (Fig. 3a). The microsphere surface is relatively rough, seen from more magnified TEM images (Fig. 3b), which is in agreement with the results reported in ref. 4. Interestingly, as for Fe_3O_4@mSiO_2-NHC(1), uniform microspheres with a good dispersion are clearly observed, and the particle diameter undergoes an apparent increase (*ca.* 80–100 nm) in comparison with the Fe_3O_4 microspheres. A gray layer around the black Fe_3O_4 core appears (Fig. 3c) and its surface become smoother than that of the Fe_3O_4 microspheres. Most of the Fe_3O_4 cores are effectively encapsulated by an organosilica layer. In the more magnified TEM images (Fig. 3d), the pores of *ca.* 2 nm in size around the core can be observed. It is worthwhile to note that most of channels in the shell are orientated to core boundary and shell outer-surface in spite of some distortions of the pore channels in comparison with a typical MCM-41 structure. Such pores perpendicular to outer surface

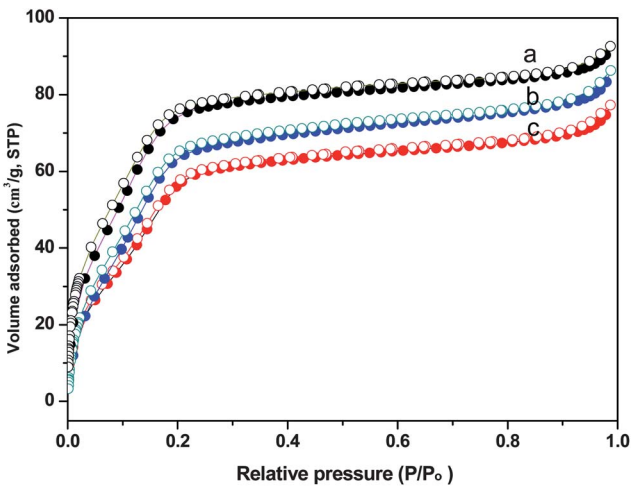

Fig. 1 N_2 adsorption/desorption isotherms of the synthesized samples: (a) Fe_3O_4@mSiO_2-NHC(1); (b) Fe_3O_4@mSiO_2-NHC(2); and (c) Fe_3O_4@mSiO_2-NHC(3).

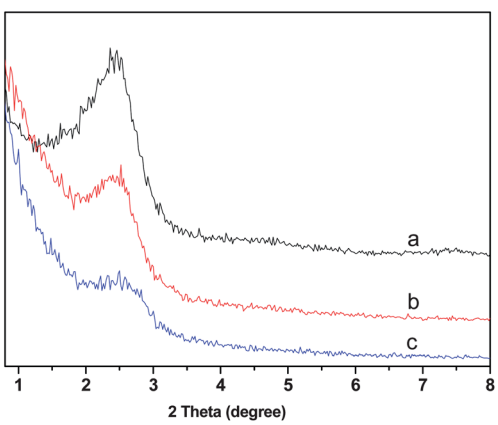

Fig. 2 XRD patterns of the synthesized samples: (a) Fe_3O_4@mSiO_2-NHC(1); (b) Fe_3O_4@mSiO_2-NHC(2); and (c) Fe_3O_4@mSiO2-NHC(3).

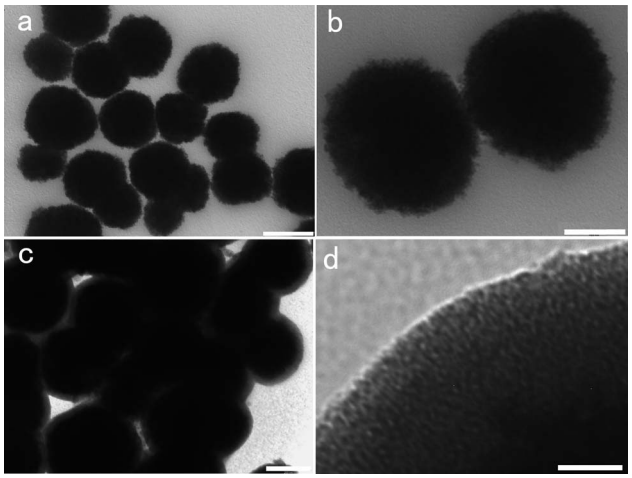

Fig. 3 TEM images of the synthesized samples: (a) Fe_3O_4, the bar is 300 nm; (b) Fe_3O_4, magnified, the bar is 100 nm; (c) Fe_3O_4@$mSiO_2$-NHC(1), the bar 200 nm; (d) Fe_3O_4@$mSiO_2$-NHC(1), magnified, the bar is 20 nm.

are favorable to a fast mass transport of reactant and product molecules.

The magnified TEM images of silica-coated Fe_3O_4 before and after encapsulation by the nanoporous organosilica shell are presented in Fig. 4. The layer thickness of silica-coated Fe_3O_4 is not identified because the layer is very thin (Fig. 4a). The shell thickness of most of the Fe_3O_4@$mSiO_2$-NHC(1) particles is estimated to be 40–50 nm from the TEM images (Fig. 4b). Consistent with N_2 sorption and XRD results, the TEM observations further confirm that Fe_3O_4@$mSiO_2$-NHC(1) indeed possesses a core–nanoporous shell structure. Moreover, as the amount of the added siliceous precursor decreases, the shell thickness decreases. The shell thickness for most of the Fe_3O_4@$mSiO_2$-NHC(2) and Fe_3O_4@$mSiO_2$-NHC(3) particles decreases down to *ca.* 30–40 and 20–30 nm, respectively (Fig. 4c and d). This trend coincides with the N_2 sorption and XRD results.

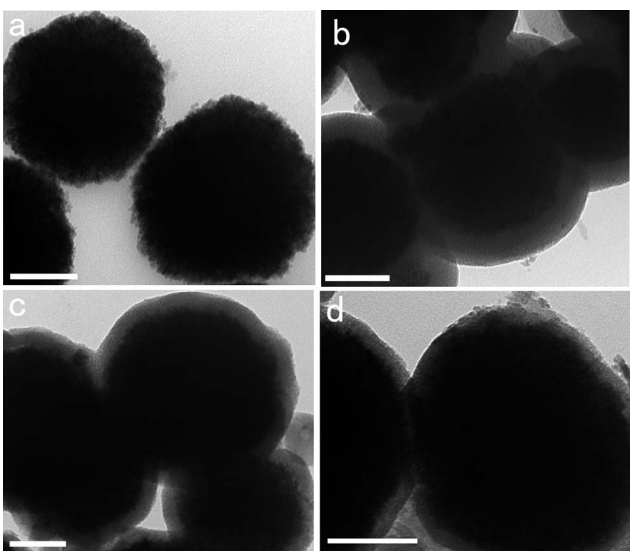

Fig. 4 TEM images of the synthesized samples: (a) SiO_2-coated Fe_3O_4; (b) Fe_3O_4@$mSiO_2$-NHC(1); (c) Fe_3O_4@$mSiO_2$-NHC(2); (d) Fe_3O_4@$mSiO_2$-NHC(3). The bar is 100 nm.

Compositional characterization

To clarify the compositions of the synthesized materials, we employed FT-IR to characterize the synthesized samples (Fig. 5). The prepared magnetic particles show a typical FT-IR spectrum of Fe_3O_4. After coating with a thin layer of SiO_2, two new peaks at 1080 and 960 cm^{-1} appear which are assigned to Si–O–Si and Si–OH stretching vibrations, respectively. Notably, Fe_3O_4@$mSiO_2$-NHC(1) exhibits new peaks at 2976, 1542 and 1468 cm^{-1} when compared with SiO_2-caoted Fe_3O_4. These three peaks are related to C–H stretching vibrations and vibrations of the NHC precursor, suggesting that the NHC precursor has been successfully integrated into the solid materials. Moreover, for Fe_3O_4@$mSiO_2$-NHC(2) the intensities of these three peaks decrease. The further decrease in the peak intensity is observed for the Fe_3O_4@$mSiO_2$-NHC(3) sample. This trend reflects the fact that the amount of siliceous material present (including NHC) decreases, which is in agreement with the amount of precursor used in the third step of the reaction.

Magnetic properties

Fig. 6 shows the wide angle XRD patterns of Fe_3O_4 and Fe_3O_4@$mSiO_2$-NHC(1). These two samples show the same diffraction peaks at 2θ = 30.1, 35.6, 43.1, 53.5, 57.1 and 62.7, which correspond to the (220), (311), (400), (422), (511) and (440) lattice planes of a typical Fe_3O_4 structure. Fe_3O_4@$mSiO_2$-NHC(1) is easily isolated magnetically by placing a magnet beside the reaction vessel wall. At the same time, this material can re-disperse into the reaction medium when the external magnet is removed (a negligible magnetic hysteresis loop at room temperature). As expected, Fe_3O_4@$mSiO_2$-NHC(1) has a good magnetization that can be inferred from the magnetic field dependence of the magnetization displayed in Fig. 7. The magnetization saturation values of Fe_3O_4, Fe_3O_4@$mSiO_2$-NHC(1), Fe_3O_4@$mSiO_2$-NHC(2) and Fe_3O_4@$mSiO_2$-NHC(3) were estimated to be 52.2, 21.9, 28.1, and 34.1 emu g^{-1} from the

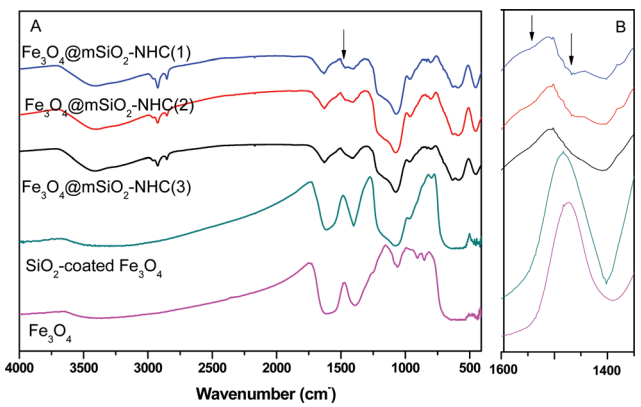

Fig. 5 FT-IR spectra of the synthesized samples (A) and regional spectra (B).

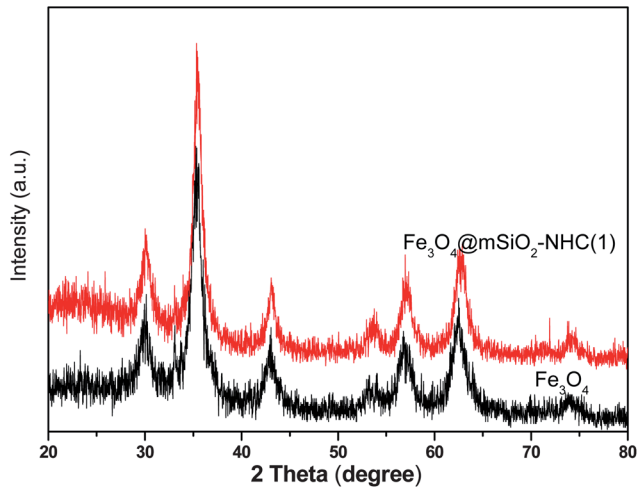

Fig. 6 Wide angle XRD patterns of Fe_3O_4 and Fe_3O_4@$mSiO_2$-NHC(1).

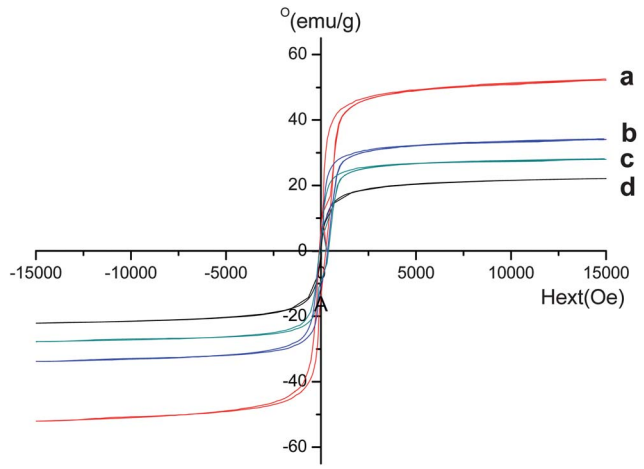

Fig. 7 Magnetization curves of the samples at 298 K: (a) Fe_3O_4; (b) Fe_3O_4@$mSiO_2$-NHC(3); (c) Fe_3O_4@$mSiO_2$-NHC(2); and (d) Fe_3O_4@mSiO2-NHC(1).

magnetization curves, respectively. Such magnetizations are sufficient for performing magnetic separation. From the change in magnetization saturation value, it can be deduced that the weight fraction of the organosilica layer (including the NHC units and nonporous silica layer) in Fe_3O_4@$mSiO_2$-NHC(1), Fe_3O_4@$mSiO_2$-NHC(2) and Fe_3O_4@$mSiO_2$-NHC(3) correspond to 58%, 46% and 35%. The decrease in the weight fraction is the consequence of reducing the total amount of siliceous precursor.

Coordination capacity

To probe the coordination capacity of *N*-heterocyclic carbene (NHC) in the solid framework of the shell, we chose $Pd(acac)_2$ to coordinate with the hybrid material because the formed Pd(NHC)(acac)Cl is stable in air and catalytically active for the Suzuki–Miyaura reaction.[13] 0.63 wt% $Pd(acac)_2$ with respect to Fe_3O_4@$mSiO_2$-NHC(1) was used. The coordination was carried out in a 1,4-dioxane solution under reflux conditions. The amount of Pd present on Fe_3O_4@$mSiO_2$-NHC(1) was determined with ICP-AES to be 0.22 wt%, which was approximately equal to the theoretic value. This reveals that the all the $Pd(acac)_2$ in solution was loaded onto Fe_3O_4@$mSiO_2$-NHC(1) under the investigated conditions. The complete coordination confirms the good ability of Fe_3O_4@$mSiO_2$-NHC(1) in coordination with metals. XPS spectroscopy was also employed to check the surface elements and the valence states of Pd species on the organosilica surface (Fig. 8). The XPS elemental survey scan of the surface of the Pd-coordinated Fe_3O_4@$mSiO_2$-NHC(1) reveals that silicon, oxygen, carbon, nitrogen and palladium are present in the material, as initially expected (Fig. 8a). However, iron, solely belonging to the core, was also detected although its intensity was very low. The XPS technique is used for surface inspection and its detection depth is usually *ca.* 10 nm, which is much less than the shell thickness. The presence of a weak signal from iron probably indicates that some of the cores were not fully

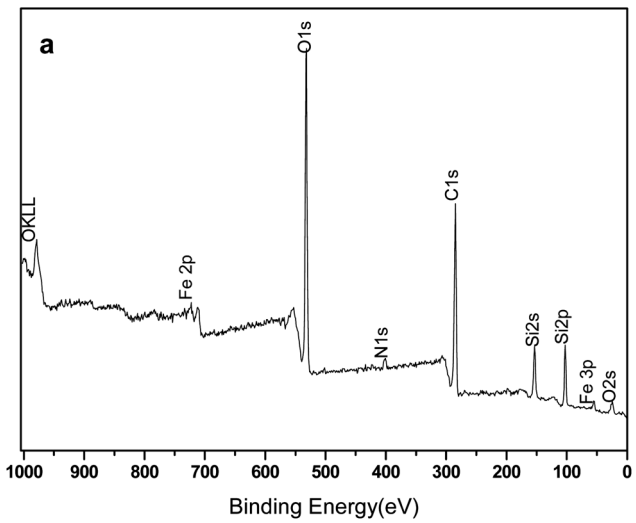

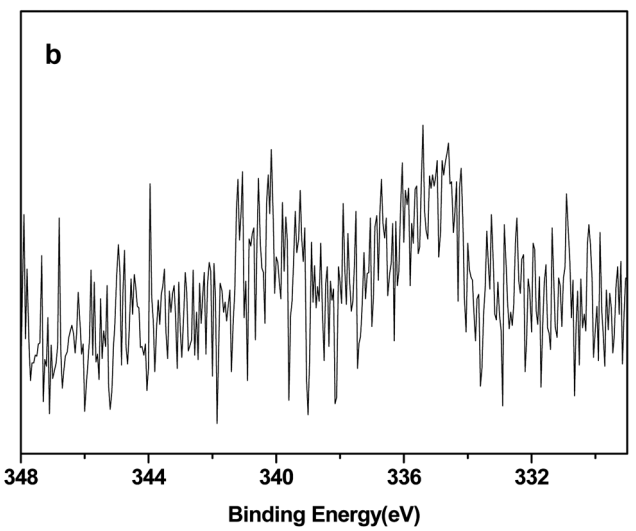

Fig. 8 XPS spectra: (a) the elemental survey scan of Fe_3O_4@$mSiO_2$-NHC(1); (b) Pd XPS regional spectra of Fe_3O_4@$mSiO_2$-NHC(1).

encapsulated by an organosilica shell. Fluorine and sulfur pertaining to trifluoromethane sulfonate ($CF_3SO_3^-$) groups of the NHC-bridged organosilane were not found. It is likely that the trifluoromethane sulfonate ($CF_3SO_3^-$) groups of the NHC precursor were exchanged by OH^- during the alkali-assisted sol–gel process. In Fig. 8b, the regional XPS spectrum of Fe_3O_4@mSiO_2-NHC(1) exhibits two peaks centered at 335.2 and 341.1 eV, which are assigned to Pd(0) $3d_{5/2}$, and Pd(0) $3d_{3/2}$, respectively. Based on these results, we speculate that Pd(0) species are formed on the surface of Fe_3O_4@mSiO_2-NHC(1) during the coordination process even though a Pd(II) precursor was employed. These results are different from our previous observation that Pd(II) complexes were yielded on a NHC-functionalized material synthesized under the acidic conditions.

Catalytic performances

To investigate the catalytic activities of the synthesized materials, we coordinated Fe_3O_4@mSiO_2-NHC(2) and Fe_3O_4@mSiO_2-NHC(3) with a given amount of $Pd(acac)_2$ along with Fe_3O_4@mSiO_2-NHC(1) (the molar ratio of NHC to Pd was kept at the same level). Their catalytic activities were evaluated with the Suzuki–Miyarura coupling of chlorobenzene and phenylboronic acid in *iso*-propyl alcohol at 80 °C under a N_2 atmosphere. Potassium *tert*-butoxide was used as a base to promote this reaction. The ratio of Pd to chlorobenzene was kept at 0.5 mol% for all the reactions. The reaction results are reflected in Fig. 9. Fe_3O_4@mSiO_2-NHC(1) gave a 63% conversion within 8 h, whereas Fe_3O_4@mSiO_2-NHC(2) and Fe_3O_4@mSiO_2-NHC(3) afforded 59% and 56% conversions, respectively. It seems contrary to our initial expectation that catalytic activity should increase with decreasing the shell thickness because of the decreased diffusion depth. Considering the unique structure and composition of Fe_3O_4@mSiO_2-NHC(x), it is not surprising because $Pd(acac)_2$ can coordinate with the nonporous SiO_2 surface and naked Fe_3O_4 surface as well as the NHC units. ICP-AES analyses confirmed our assumption that SiO_2-encapsulated Fe_3O_4 could indeed also capture $Pd(acac)_2$ form the solution. 0.083 wt% Pd was detected on SiO_2-encapsulated Fe_3O_4 that was

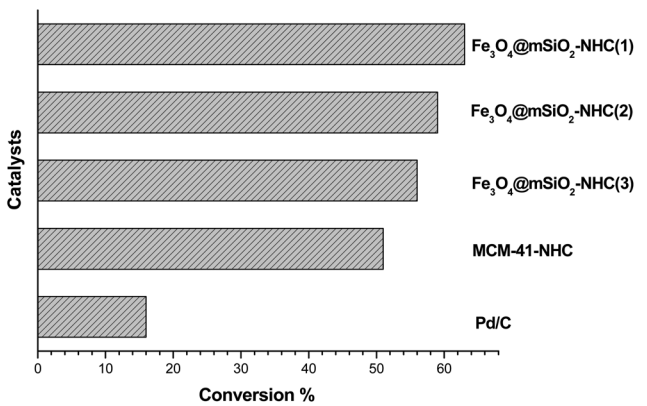

Fig. 9 The chlorobenzene conversions over different solid catalysts. Reaction conditions: aryl chlorides (1 mmol), phenylboronic acid (1.1 mmol), potassium *tert*-butoxide (1.5 mmol) and *iso*-propyl alcohol (3 mL), and the solid catalyst (0.5 mol% with respect to aryl chlorides), 80 °C, 8 h, under a N_2 atmosphere.

treated with $Pd(acac)_2$ using the same procedure as Fe_3O_4@mSiO_2-NHC(1). The Pd sites-related pure SiO_2 and Fe_3O_4 are both almost inactive in the Suzuki–Miyarura coupling of chlorobenzene. As the shell thickness decreases, the fraction of active Pd site decreases and the fraction of inactive Pd sites increases, thus leading to the decrease in the activity.

In order to further evaluate the performance of this catalyst, we compared the activity of Fe_3O_4@mSiO_2-NHC(1) with that of NHC-functionalized MCM-41 microspheres that were synthesized under the same conditions except without the addition of the Fe_3O_4 cores (its TEM images and XRD pattern were included in Fig. S1 and Fig. S2 in the ESI†). Under the same conditions, NHC-functionalized MCM-41 microspheres gave a conversion of 51%. It is much lower than Fe_3O_4@mSiO_2-NHC(1) although Fe_3O_4@mSiO_2-NHC(1) included a fraction of inactive Pd sites. The comparison suggests activity enhancement effects caused by a core–shell structure. The enhanced activity may be attributed to the significantly reduced diffusion pathway because the catalytic reaction solely occurs in outer nanoporous shell of Fe_3O_4@mSiO_2-NHC(1), not throughout the whole microspheres of NHC-functionalized MCM-41. Impressively, under identical reactions conditions, commercial Pd/C (with a Pd loading of 1 wt%) gave a conversion of only 16%, which was also much lower than Fe_3O_4@mSiO_2-NHC(1). These striking contrasts further highlight the superiority of Fe_3O_4@mSiO_2-NHC(1). Several types of heterogeneous catalysts for Suzuki–Miyaura couplings were reported such as Pd/C, mesoporous silica-supported palladium, polymer-incarcerated palladium, polyurea-encapsulated palladium and dendrimer-supported palladium catalysts.[14] These heterogeneous systems successfully catalyzed the Suzuki–Miyaura couplings of aryl bromides but failed in the couplings of aryl chlorides except in only limited examples.[10] In this context, our developed catalyst Fe_3O_4@mSiO_2-NHC(1) outperforms most of the reported heterogeneous catalysts in the terms of activity and catalyst recovery. The high activity is attributed to a favorable combination of the presence of a molecularly functional moiety only in the shell, decreased diffusion length as well as the radially aligned pore architecture.

To further evaluate the catalytic performances of the Pd-coordinated Fe_3O_4@mSiO_2-NHC(1), Suzuki–Miyaura couplings of various arylboronic acids and chlorobenzene were conducted using *iso*-propyl alcohol as the solvent at 80 °C under a N_2 atmosphere (Table 2). At a Pd loading of 0.5 mol%, for phenylboronic acids, the Pd-coordinated Fe_3O_4@mSiO_2-NHC(1) gave a 73% yield within 12 h (Table 2, entry 1). 73% and 72% yields were achieved in the cases of arylboronic acids bearing electron-donating methyl and *tert*-butyl groups (Table 2, entries 2 and 3). The moderately sterically demanding arylboronic acids were also smoothly converted to the corresponding products in 70–86% yields (Table 2, entries 4 and 5). For fluoro-substituted arylboronic acid, 69% yield was achieved (Table 2, entry 6). Aryl boronic acid bearing strong electron-withdrawing groups needs a relatively longer time to obtain a moderate yield (Table 2, entry 7).

Encouraged by the impressive results for the Suzuki–Miyaura couplings of chlorobenzene and boronic acids, we wanted to test the catalytic activity towards the couplings of benzylic chloride and arylboronic acids because this coupling reaction provids an important alternative to the Friedel–Crafts reaction for synthesis

Table 2 The Suzuki–Miyaura couplings of various phenylboronic acids and chlorobenzene over the Pd-coordinated Fe_3O_4@mSiO_2-NHC(1)

Entry	Substrates	Products	Time (h)	Yield[a] (%)
1	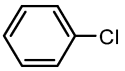	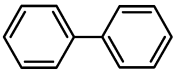	12	73
2	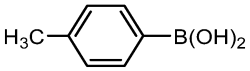	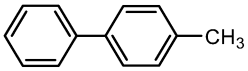	12	73
3	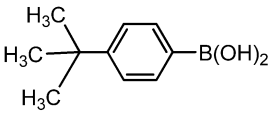	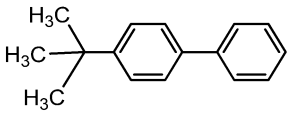	12	72
4	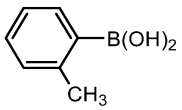	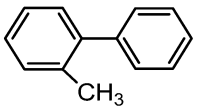	12	63
5	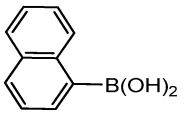	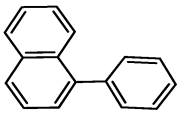	12	79
6	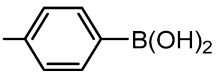	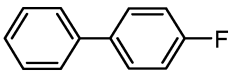	12	69
7	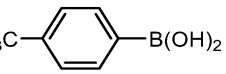	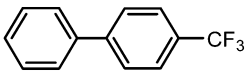	24	59

[a] Isolated yields.

of diarylmethane-type aromatics.[15] Using phenylboronic acid as a substrate, the Pd-coordinated Fe_3O_4@mSiO_2-NHC(1) gave diphenylmethane in a yield up to 79% (Table 3, entry 1). In followed reactions, in spite of electron-rich arylboronic acids (Table 3, entries 2–7) and electron-poor arylboronic acid (Table 3, entry 8), various diarylmethane compounds in 71–89% yields could be obtained.

The recyclability of the Pd-coordinated Fe_3O_4@mSiO_2-NHC(1) was investigated with the consecutive Suzuki–Miyaura reactions of chlorobenzene with phenylboronic acid (Table 4).The fresh solid catalyst gave the product in a 73% yield within 12 h. After the first reaction cycle, the catalyst could be separated with the reaction liquid by using an external magnetic field (Fig. S3 in the ESI†). The magnetic separation was easy, fast and clean, avoiding the need for centrifugation and filtration that require extra energy. After the reaction liquid was removed, diethyl ether and acetone in sequence were added to wash the recovered solid catalyst. After washing and drying, the recovered catalyst was directly used for the next reaction cycle. For the second and third reaction cycles, yields greater than 69% were achieved within the same number of hours as the first run. From the fourth reaction cycle, the activity of the reused catalyst was observed to slightly decrease. A 57% yield was obtained within 15 h. For the fifth reaction cycle, a reaction time of 20 h led to a 51% yield and the prepared catalyst could still separated with a magnet. The good recyclability may be attributable to the NHC-functionalized nanopores that can efficiently prevent the aggregation or agglomeration of Pd nanoparticles through the spatial restrictions imposed by nanopores and electrostatic interactions with the NHC unit on the nanopore surface.[7d]

To check the reaction nature, namely heterogeneous catalysis and homogeneous catalysis, we tested the activity of the filtrate of the catalytic reaction. After the coupling reaction of chlorobenzene with phenylboronic acid had proceeded for 6 h (with conversion at 54%) the reaction was stopped and the filtrate was immediately collected under the hot conditions. A further 5% increase in conversion was observed after heating the filtrate at 80 °C for another 4 h (50% of the initial amount of potassium *tert*-butoxide was added to the filtrate). These results may indicate that the observed conversion was at least partially contributed to by leached Pd species in the filtrate. The Pd loss may be attributed to two factors. One is related to the Pd leaching from the solid catalyst during catalytic reaction. The other results from the brushing off of the nanoporous organosilica layer from the magnetic core (Si was detected in the filtrate by ICP-AES) because of the persistent stirring during reaction, yielding fine particles

Although the activity of the solid catalyst decreases during the consecutive recycling reactions, it represents a highly recoverable heterogeneous catalyst for the Suzuki–Miyaura coupling of less reactive aryl chlorides, considering a relatively low Pd loading (0.5 mol%). Additionally, this solid catalyst exhibited a high stability in air. It was found that there was no decrease in activity and magnetic isolation ability even after the catalyst was exposed to air for several days. In this aspect, the developed catalyst is also superior to immobilized phosphine catalysts.

Table 3 The coupling reactions of benzylic chloride and various arylboronic acids over the Pd-coordinated Fe_3O_4@mSiO$_2$-NHC(1)

Entry	Arylboronic acids	Products	Time (h)	Yield[a] (%)
1	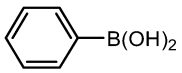	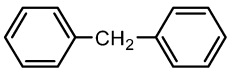	8	79
2	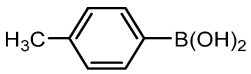	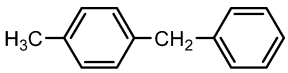	8	80
3	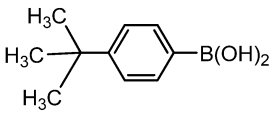	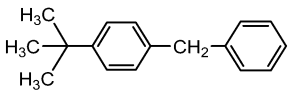	10	71
4	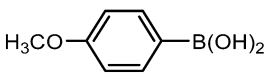	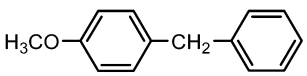	8	81
5	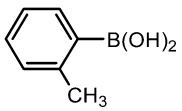	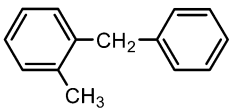	8	89
6	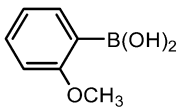	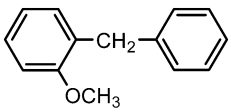	8	73
7	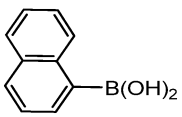	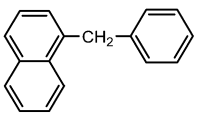	8	85
8	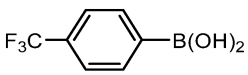	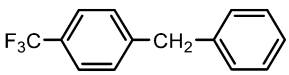	10	71

[a] Isolated yield.

Table 4 Recyclability test of the Pd-coordinated Fe_3O_4@mSiO$_2$-NHC(1) for the Suzuki–Miyaura coupling reaction

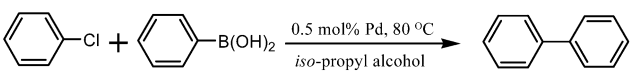

Cycles	1	2	3	4	5
Time (h)	12	12	12	15	20
Yield[a] (%)	73	75	69	57	51

[a] Isolated yield.

Conclusions

We report a successful synthesis of magnetic core–shell-structured nanoporous organosilica microspheres with built-in NHC ligands by growing a layer of NHC-functionalized nanoporous organosilica around a Fe_3O_4 core with the aid of a template. These microspheres thus-obtained have nanopores (1.6 nm) in the shell, moderate surface area, uniform morphology and high magnetization. The growth of a nanoporous organosilica shell with controlled thickness around Fe_3O_4 can be achieved by varying the amount of siliceous precursor added. Such multifunctional materials exhibit a good coordination ability toward Pd. The Pd-coordinated material was highly active toward the Suzuki–Miyaura coupling of less active aryl chlorides, and its activity was found to be dependent on the organosilica shell thickness. Impressively, the resultant catalyst showed activity enhancement effects in comparison with the analogous MCM-41 microspheres due to the significantly decreased diffusion depth. Furthermore, the developed catalysts can be easily isolated by using a magnetic field and directly used in the next reaction cycles without a significant loss of its activity, suggesting promising application potentials. This study, other than supplying a novel synthesis of magnetic core–shell structured nanoporous organosilica microspheres with molecular functionalization, demonstrates the catalytic activity enhancement effects, which is crucial for designing high-performance solid catalysts.

Acknowledgements

We acknowledge Specialized Research Fund for the Doctoral Program of Higher Education (200801081035), Shanxi Natural Science Foundation for Youths (2009021009) and the Natural Science Foundation of China (20903064, 21173137).

References

1 (*a*) F. Caruso, R. A. Caruso and H. Möhwald, *Science*, 1998, **282**, 1111; (*b*) L. M. Liz-Marzán, M. Giersig and P. Mulvaney, *Langmuir*, 1996, **12**, 4329; (*c*) Z. H. Xu, Y. L. Hou and S. H. Sun,

J. Am. Chem. Soc., 2007, **129**, 8698; (*d*) Y. H. Deng, W. L. Yang, C. C. Wang and S. K. Fu, *Adv. Mater.*, 2003, **15**, 1729; (*e*) C. Graf, D. L. J. Vossen, A. Imhof and A. van Blaaderen, *Langmuir*, 2003, **19**, 6693; (*f*) L. Zhang, S. Z. Qiao, Y. G. Jin, H. G. Yang, S. Budihartono, F. Stahr, Z. F. Yan, X. L. Wang, Z. P. Hao and G. Q. Lu, *Adv. Funct. Mater.*, 2008, **18**, 3203; (*g*) W. Schäartl, *Nanoscale*, 2010, **2**, 829; (*h*) C. J. Zhong and M. M. Maye, *Adv. Mater.*, 2001, **13**, 1507; (*i*) D. C. Niu, Z. Ma, Y. S. Li and J. L. Shi, *J. Am. Chem. Soc.*, 2010, **132**, 15144.

2 (*a*) Z. H. Xu, C. X. Li, X. J. Kang, D. M. Yang, P. P. Yang, Z. Y. Hou and J. Lin, *J. Phys. Chem. C*, 2010, **114**, 16343; (*b*) E. Katz and I. Willner, *Angew. Chem., Int. Ed.*, 2004, **43**, 6042; (*c*) Y. H. Deng, D. W. Qi, C. H. Deng, X. M. Zhang and D. Y. Zhao, *J. Am. Chem. Soc.*, 2008, **130**, 28; (*d*) L. Zhang, S. Z. Qiao, Y. G. Jin, Z. G. Chen, H. C. Gu and G. Q. Lu, *Adv. Mater.*, 2008, **20**, 805; (*e*) J. Liu, Z. K. Sun, Y. H. Deng, Y. Zou, C. Y. Li, X. H. Guo, L. Q. Xiong, Y. Gao, F. Y. Li and D. Y. Zhao, *Angew. Chem., Int. Ed.*, 2009, **48**, 5875; (*f*) E. Katz and I. Willner, *Angew. Chem., Int. Ed.*, 2004, **43**, 6042; (*g*) C. Q. Yang, G. Wang, Z. Y. Lu, J. Sun, J. Q. Zhuang and W. S. Yang, *J. Mater. Chem.*, 2005, **15**, 4252; (*h*) Y. Yang, J. Liu, X. B. Li, X. Liu and Q. H. Yang, *Chem. Mater.*, 2011, **23**, 3676; (*i*) J. Liu, S. Z. Qiao, Q. H. Hu and G. Q. Lu, *Small*, 2011, **7**, 425; (*j*) J. Liu, B. Wang, S. B. Hartono, T. Liu, P. Kantharidis, A. P. J. Middelberg, G. Q. Lu, L. He and S. Z. Qiao, *Biomaterials*, 2012, **33**, 970.

3 W. R. Zhao, J. L. Gu, L. X. Zhang, H. R. Chen and J. L. Shi, *J. Am. Chem. Soc.*, 2005, **127**, 8916.

4 Y. H. Deng, Y. Cai, Z. K. Sun, J. Liu, C. Liu, J. Wei, W. Li, C. Liu, Y. Wang and D. Y. Zhao, *J. Am. Chem. Soc.*, 2010, **132**, 8466.

5 J. P. Ge, Q. Zhang, T. R. Zhang and Y. D. Yin, *Angew. Chem., Int. Ed.*, 2008, **47**, 8924.

6 (*a*) S. Inagaki, S. Guan, Y. Fukushima, T. Ohsuna and O. Terasaki, *J. Am. Chem. Soc.*, 1999, **121**, 9611; (*b*) T. Asefa, M. J. MacLachlan, N. Coombs and G. A. Ozin, *Nature*, 1999, **402**, 867; (*c*) B. J. Melde, B. T. Holland, C. F. Blanford and A. Stein, *Chem. Mater.*, 1999, **11**, 3302; (*d*) Y. Wan, D. Q. Zhang, Y. P. Zhai, C. M. Feng, J. Chen and H. X. Li, *Chem.–Asian J.*, 2007, **2**, 875.

7 (*a*) A. Corma, D. Das, H. García and A. Leyva, *J. Catal.*, 2005, **229**, 322; (*b*) P. Y. Wang, X. Liu, J. Yang, Y. Yang, L. Zhang, Q. H. Yang and C. Li, *J. Mater. Chem.*, 2009, **19**, 8009; (*c*) H. Q. Yang, G. Li, Z. C. Ma, J. B. Chao and Z. Q. Guo, *J. Catal.*, 2010, **276**, 123; (*d*) H. Q. Yang, X. J. Han, G. Li, Z. C. Ma and Y. J. Hao, *J. Phys. Chem. C*, 2010, **114**, 22221; (*e*) H. Q. Yang, Y. W. Wang, Y. Qin, Y. Z. Chong and Q. Z. Yang, *Green Chem.*, 2011, **13**, 1352; (*f*) W. J. Hunks and G. A. Ozin, *J. Mater. Chem.*, 2005, **15**, 3716; (*g*) F. Hoffmann, M. Cornelius, J. Morell and M. Frçba, *Angew. Chem., Int. Ed.*, 2006, **45**, 3216; (*h*) S. Fujita and S. Inagaki, *Chem. Mater.*, 2008, **20**, 891; (*i*) P. Nguyen, P. Hesemann, P. Gaveau and J. J. E. Moreau, *J. Mater. Chem.*, 2009, **19**, 4164.

8 (*a*) C. Li, *Catal. Rev. Sci. Eng.*, 2004, **46**, 419; (*b*) H. Q. Yang, J. Li, J. Yang, Z. M. Liu, Q. H. Yang and C. Li, *Chem. Commun.*, 2007, 1086.

9 (*a*) N. Miyaura, T. Yanagi and A. Suzuki, *Synth. Commun.*, 1981, **11**, 513; (*b*) J. S. Carey, D. Laffan, C. Thomson and M. T. Williamsd, *Org. Biomol. Chem.*, 2006, **4**, 2337; (*c*) M. Lamblin, L. Nassar-Hardy, J. C. Hierso, E. Fouquet and F. X. Felpin, *Adv. Synth. Catal.*, 2010, **352**, 33.

10 (*a*) M. J. Jin and D. H. Lee, *Angew. Chem., Int. Ed.*, 2010, **49**, 1119; (*b*) D. H. Lee, J. Y. Jung and M. J. Jin, *Green Chem.*, 2010, **12**, 2024.

11 J. Liu, Z. K. Sun, Y. H. Deng, Y. Zou, C. Y. Li, X. H. Guo, L. Q. Xiong, Y. Gao, F. Y. Li and D. Y. Zhao, *Angew. Chem., Int. Ed.*, 2009, **48**, 5875.

12 D. C. Niu, Z. Ma, Y. S. Li and J. L. Shi, *J. Am. Chem. Soc.*, 2010, **132**, 15144.

13 N. Marion, P. D. Frémont, I. M. Puijk and E. C. Ecarnot, *Adv. Synth. Catal.*, 2007, **349**, 2380.

14 D. H. Lee, J. H. Kim, B. H. Jun, H. Kang, J. Park and Y. S. Lee, *Org. Lett.*, 2008, **10**, 1609 and references therein.

15 (*a*) M. J. Burns, I. J. S. Fairlamb, A. R. Kapdi, P. Sehnal and R. J. K. Taylor, *Org. Lett.*, 2007, **9**, 5397; (*b*) B. P. Bandgar, S. V. Bettigeri and J. Phopase, *Tetrahedron Lett.*, 2004, **45**, 6959.

